論文 / 著書情報
Article / Book Information

Title	Ultra-compact VCSEL scanner for high power solid-state beam steering
Authors	SHANTING HU, XIAODONG GU, AHMED HASSAN, RUIXIAO LI, MASANORI NAKAHAMA, SATOSHI SHINADA, FUMIO KOYAMA
Citation	Optics Express, Vol. 30, No. 6, pp. 8742-8749 (2022)
Pub. date	2022, 3
Copyright	(c) 2022 Optical Society of America. Users may use, reuse, and build upon the article, or use the article for text or data mining, so long as such uses are for non-commercial purposes and appropriate attribution is maintained. All other rights are reserved.
DOI	http://dx.doi.org/10.1364/OE.453090

Research Article | Vol. 30, No. 6 / 14 Mar 2022 / Optics Express 8742

Optics EXPRESS

Ultra-compact VCSEL scanner for high power solid-state beam steering

SHANTING HU,[1,2,*] XIAODONG GU,[1,3] AHMED HASSAN,[1,4] RUIXIAO LI,[1] MASANORI NAKAHAMA,[1,3] SATOSHI SHINADA,[5] AND FUMIO KOYAMA[1]

[1]*Institute of Innovative Research (IIR), Tokyo Institue of Technology, 4259 Nagatsuta, Midori-ku Yokohama,226-8503, Japan*
[2]*School of Information and Electronics, Beijing Institue of Technology, No. 5 Yard, Zhong Guan Cun South Street, Haidian District, Beijing, China*
[3]*Ambition Photonics Inc., Tokyo Tech Yokohama Venture Plaza E208, Yokohama 226-8510, Japan*
[4]*Department of Physics, Faculty of Science, Al-Azhar University, Assuit, Egypt*
[5]*National Institute of Information and Communications Technology, Japan*
[*]*hu.s.ab@m.titech.ac.jp*

Abstract: We demonstrate the lateral monolithic integration of a tunable first-order surface-grating loaded vertical-cavity surface-emitting laser (VCSEL) and slow-light waveguide with fan-beam steering and amplifier function. Shallow Bragg-grating formed on the surface of a VCSEL section enables the selection of a single slow-light mode, which can be coupled into the integrated long waveguide and amplified through pumping the amplifier above threshold. We obtained over 3W amplified slow-light power with single-mode operation and over 4W amplified quasi-single-mode power under pulsed current injection. To the best of our knowledge, this is the highest output power for single-mode VCSELs. Solid-state beam steering of the device is also demonstrated with 9° fan-beam steering range and 200 resolution points.

1. Introduction

VCSELs are extensively applied in short range data communications due to its unique advantages including low manufacturing cost, low-power consumption, high reliability and so on [1–5]. After years of research and developments, VCSELs are also commonly deployed in various applications including laser manufacturing, laser printers and medical imaging [6–9]. 3D sensing including LiDARs and 3D camera in smart phones has garnered more and more attention recently. However, to achieve solid state beam steering with both good beam quality and high power for VCSELs to satisfy the demand of solid-state LiDARs comes as a big challenge. Flash LiDARs based on a two-dimensional VCSEL array is considered as one possible solution thanks to its high pulsed peak power at kW-class, but its poor beam quality comes across as a problem [10–13]. Extra optical elements are needed to converge the beam divergence angle, adding cost and complexity to the overall solution. There has been research on solid state beam scanner based on silicon-on-insulator optical phased arrays [14,15]. However, due to the low tuning efficiency which is around 0.14 °/nm, extra wide range tunable laser source is needed. Photonic crystal surface emitting laser was also explored for its beam steering operation [16,17]. Oblique-angle emission was achieved through manipulating the lasing band edge with selective current injection at different electrodes on the device surface. However, the number of resolution points is limited below 100 and an electric circuit is needed to balance injected currents of the neighboring electrodes for continuous beam steering [17].

In our previous research, we proposed a slow-light VCSEL amplifier [18,19] and demonstrated its beam scanning and amplification function [20,21]. 27° beam steering range with 600 resolution points and 3W single-mode power are achieved [22]. Also, with adding a diffractive optical

#453090 https://doi.org/10.1364/OE.453090
Journal © 2022 Received 18 Jan 2022; revised 16 Feb 2022; accepted 21 Feb 2022; published 1 Mar 2022

Optics EXPRESS

element (DOE), we obtained over 4,000 resolution points for fan-beam steering [23]. However, an external tunable laser is needed for the electrical beam steering function. Thus, the monolithic integration of a tunable laser becomes a key challenge. We demonstrated a tunable VCSEL integrated beam scanner with a design of resonant wavelengths detuning [24]. In the device, lasing light from the seed VCSEL is coupled laterally into the integrated beam scanner thanks to cut-off wavelength detuning between the two cavities. When we pump the amplifier above the threshold current, the coupled slow light can get amplification along the amplifier waveguide, in which case the amplified power of the light emission is in proportion to the length of the scanner and the beam divergence angle can be reduced by extending the scanner length. Thus, both high beam quality and strong power can be realized for the integrated device. However, since the coupled power from the seed laser to the scanner is restricted by the small oxidized aperture for single mode operation to around 1mW, the maximum amplified slow light power which is dependent on the coupled power according to [25] is only about 40 mW.

There has been research on a ridge-waveguide DFB laser with shallow surface gratings and oxide aperture based on GaAs/AlGaAs [26]. Lately, we reported a high power VCSEL with surface grating loaded named as "slow light laser", which demonstrates over 3W single-mode power [27,28]. When a slow light laser is utilized as a seed VCSEL for the lateral integration, the output of the seed VCSEL is greatly enhanced, which enables high coupled power from the seed VCSEL to the amplifier/beam scanner. We then reported a VCSEL beam scanner with the structure of lateral integration of a seed VCSEL with grating loaded on surface and a 2 mm waveguide, demonstrating a scan range of 1.8° and a single-mode power of 1 W [29]. However, because high order gratings were utilized in the fabrication, single-mode operation is not stable in the seed VCSEL.

In this study, a novel scheme of solid state VCSEL beam scanner with first-order surface gratings is proposed, demonstrating the record performance in both single mode power and beam steering range.

2. Device structure

The schematic diagram of the fabricated VCSEL scanner is shown in Fig. 1(a). The device is fabricated based on a conventional VCSEL structure with a vertical resonant wavelength designed at 865nm. The top DBR mirror consists of 19 pairs of p-type AlGaAs doped with carbon and the bottom DBR mirror consists of 40 Si-doped n-type pairs. The active region includes three GaAs/AlGaAs quantum wells with a gain peak wavelength of around 850 nm. The mesa structures is formed by inductively coupled plasma (ICP) etching. The current apertures are formed by wet thermal oxidation of an $Al_{0.98}Ga_{0.02}As$ layer. A VCSEL beam scanner is followed by a taper section to attenuate the reflected light at the end. A tunable single-mode seed VCSEL is laterally integrated by fabricating a surface-loaded grating at the beginning segment of the scanner. A slow light mode lases at this segment and the surface-loaded grating enables stable single slow light mode oscillation at the Bragg-wavelength [26]. The calculation of the effective index when there is a wet-etching of 30nm on the top GaAs contact layer is performed utilizing the film mode matching method. As similar to a distributed feedback laser (DFB), there is coupling between the forward and backward slow light modes and the Bragg wavelength is determined by a grating pitch Λ and phase refractive index n_{eff} in the following equation.

$$\lambda_B = 2n_{eff}/\Lambda \tag{1}$$

Thanks to the large dispersion in the slow light waveguide, the phase index n_{eff} of the designed Bragg-wavelength (850 nm) is around 0.82, which results in a rather large 1st order grating pitch around 520 nm. The pitch size of our surface relief VCSEL is 4 time larger than that of conventional guided-wave DFB lasers. Also, a shallow surface etching of 30 nm provides a coupling strength κL of 1.3 between forward and backward waves, which is large enough. Thus,

Optics EXPRESS

it is much easier to fabricate than that of conventional guided-wave DFB lasers. Figure 1(b) shows overhead view of the beam scanner fabricated in our lab. The oxide aperture width is 4 μm. The aperture length of the seed VCSEL and amplifier/beam scanner is defined by the length of the top electrode, which is 500 μm and 4 mm, respectively. Figure1 (c) shows a magnified figure of the grating part. Electron beam lithography is used to form the pattern of 520 nm-pitch grating and the grating grooves are dry-etched with a depth of 30 nm. Since the wavelength of the lasing mode selected by the gratings at Bragg-wavelength in the seed VCSEL is 15 nm smaller than the vertical cavity resonance (865 nm), the light emission angle is tilted from the vertical direction and strong lateral coupling of optical power from the seed VCSEL into the amplifier/scanner waveguide is realized.

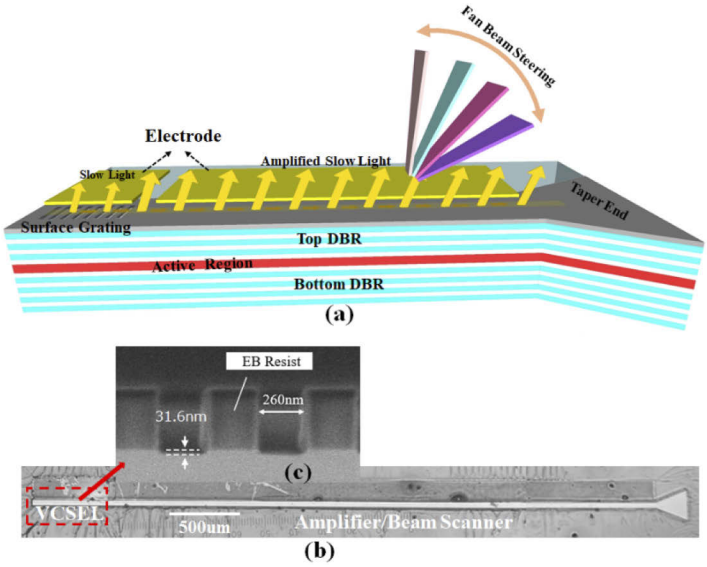

Fig. 1. (a) Schematic diagram of the integrated beam scanner (b) Overhead view of a fabricated device (c) Amplified figure of the grating part

3. Measurement setup

The measurement setup of our proposed solid-state scanner is sketched in Fig. 2. The sample is mounted on a copper stage with a temperature controller attached. Two separate probes are used to pump the seed VCSEL and beam scanner respectively. The probe for seed VCSEL is connected to a laser driver, which deliver CW current to the seed VCSEL. Another probe connected to a short pulse driver delivers 50ns pulse current to the amplifier/beam scanner. The output beam captured by the FFP measurement system is split into two to measure the spectrum with a spectrum analyzer of 0.01nm spectral resolution and far field pattern (FFP) with a FFP camera of 0.001° resolution. Because the emission of the amplified slow light from our VCSEL beam scanner shows an oblique angle, the head of the FFP measurement camera is attached to a rotation stage, which enables the FFP camera to rotate around the device. Therefore, the position adjustment of the FFP camera can be carried out to catch the tilted emission from the device. Once the emission angle of the amplified light is confirmed by the FFP image, a large area photodiode tilted at the same angle will be placed on top of the device to measure the output of the amplifier for the illustration of light-current (LI) curve.

Optics EXPRESS

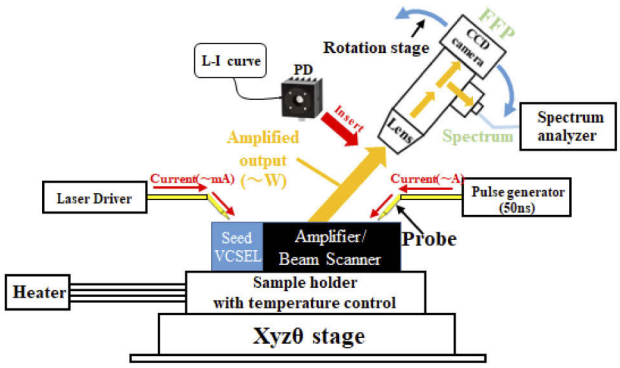

Fig. 2. Measurement setup of the fabricated VCSEL scanner

4. Experimental results and discussions

The measured spectra of the seed VCSEL under different injection currents without any pumping at the amplifier is shown as in Fig. 3(a). Single mode lasing in the slow light mode is successfully selected by the gratings with a SMSR over 40dB. As shown in the figure, the single-mode operation of the seed laser remains stable while the pump current is gradually increased. When the pump current reaches 250 mA, vertical emission starts to take place due to the red shift of the photoluminescence (PL) wavelength towards the cavity resonance of VCSEL, which limits the growth of the single slow light mode power. Figure 3(b) shows the LI curve of the seed VCSEL measured by the photodiode. As we can see in the figure, since a single mode power of 68mW for the seed VCSEL is obtained at 200mA pump current, large coupling power from the seed VCSEL to the amplifier section can be expected.

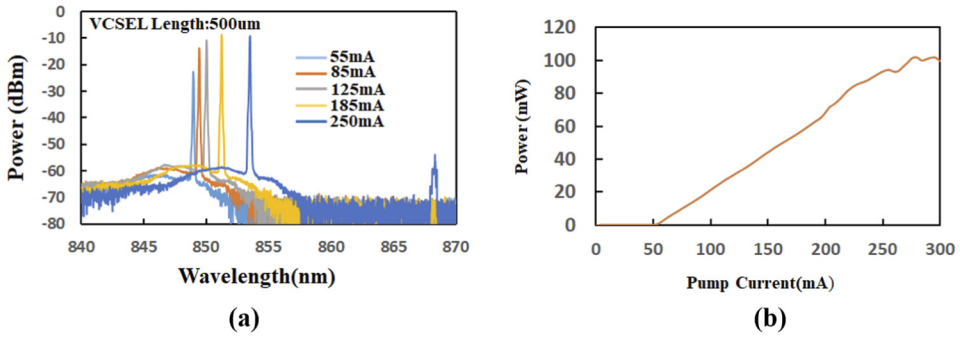

Fig. 3. (a) Measured spectra of the seed VCSEL under different pump currents. (b) Output power against the pump current of the seed VCSEL

L/I characteristic of the integrated device with both the seed VCSEL and the amplifier/scanner being pumped is shown in Fig. 4. The seed VCSEL is pumped with a CW current of 180mA and the amplifier/scanner is pumped with a high pulse current with 50ns duration to mitigate the thermal effect for high power output. To confirm the amplification of the slow light with single mode operation, spectra at different pulse current are also measured. When the amplifier/scanner is pumped with a pulse current of 6A, single mode power of over 3 W was obtained with SMSR of over 15dB as shown in Fig. 4, which is almost 1000 times larger than that of a conventional single mode VCSEL with a small oxidized aperture. When the pump current is enhanced to 7.5A,

Optics EXPRESS

amplified spontaneous emission (ASE) occurs as shown in the spectrum, due to which the SMSR is reduced to 10dB.

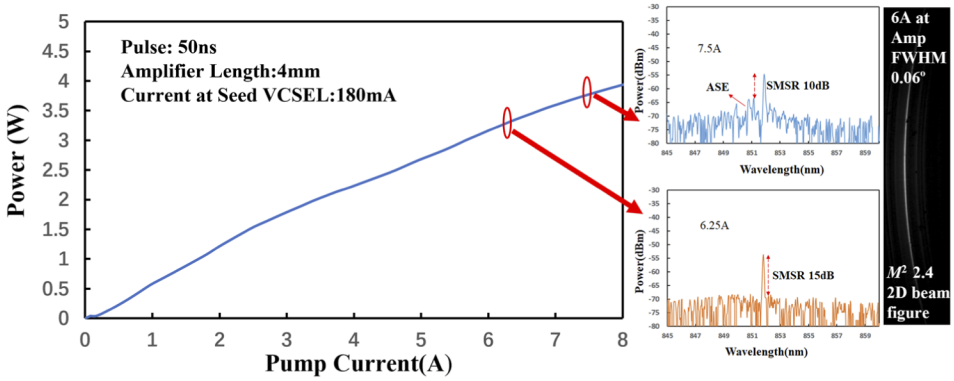

Fig. 4. Measured L/I characteristics of the integrated device under pulse operation, corresponding spectrum at 6.25A and 7.5A current pump and 2D beam figure at 6A.

We investigate the amplification characteristics of our beam scanner through the measurements of FFP with fixed CW current at the seed VCSEL and different pulsed currents at the amplifier/scanner. The results are shown in Fig. 5(a). A narrow divergence (0.06°) single-lobe FFP is achieved with a tilted angle of 49°. The peak beam intensity increases as increasing the pump current from 3A to 7A, which demonstrates the single mode amplification of our device. Corresponded to the ASE of the spectrum as shown in Fig. 4, above 7A current pump, side lobes appear around the FFP angle of 50.5°, which saturates the output power of our amplifier. The M^2 could be estimated through the measured divergence angle divided by the diffraction limitation. The diffraction limit of our 4mm device is 0.025° at a deflection angle of around 50°. The FWHM of the divergence at 3A and 6A are 0.05° and 0.06°, which provide M^2 of 2 and 2.4, respectively. The broadening of the divergence is due to the non-uniform current distribution at high currents, which could be mitigated when the wire-bonding is utilized. Also, it is noted that the M^2 in the orthogonal direction is nearly 1.0. Thus, the average M^2 in two directions could be $M_a^2 = \sqrt{2.4*1} = 1.55$.

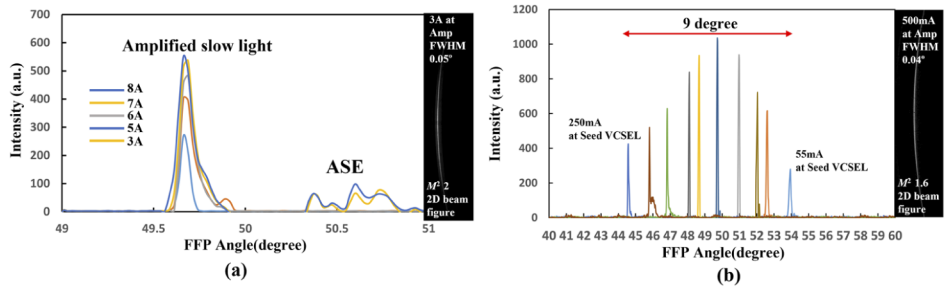

Fig. 5. (a) Measured FFP at different pulse current injections in the amplifier/scanner. (b) Measured FFP when seed laser is pumped with different current.

The electronically controlled beam-steering performance under CW operation of our integrated beam scanner is demonstrated in Fig. 5(b). Thanks to the large angular dispersion of the VCSEL scanner, when the wavelength of a seed light is varied, the deflection angle of the output beam

Optics EXPRESS

steers correspondingly as shown in Eq. (2) [20],

$$sin\theta_{out} = n_{wg}\sqrt{1 - (\frac{\lambda_{in}}{\lambda_o})^2} \tag{2}$$

θ_{out} is the beam deflection angle, $n_{wg} \approx 3.3$ is the refractive index of the amplifier/scanner waveguide, λ_{in} is the wavelength of the seed light, $\lambda_o \approx 865$nm is the resonance wavelength of the vertical cavity mode of VCSEL waveguide. Since the full scanning range of our beam scanner is 9° as shown in Fig. 5(b) and the wavelength tuning range of the seed VCSEL is around 5nm as shown in Fig. 3, the calculated wavelength-tuned steering efficiency of our beam scanner is 1.8°/nm. Continuous wavelength sweeping of the seed VCSEL can be achieved by varying injection currents due to self-heating effect. With fixing the pump current of amplifier at 500mA, continuous beam steering can be achieved with current injection controllable wavelength tuning of the seed VCSEL. The minimum full width at half maximum (FWHM) divergence angle of the beam is around 0.04°, which is comparable to the diffraction-limited angle of 0.025° for a device length of 4 mm. As can be seen in Fig. 5(a), under pulsed operations there is a broadening (0.02°) of the beam divergence angle. The divergence broadening is imposed by the heating-induced transient refractive changes of the amplifier. The whole beam scanning range is around 9° with over 200 resolution points under CW operations of the beam scanner by continuously tuning the wavelength of the seed VCSEL as shown in Fig. 2. It is noted that the intensity of the amplified output varies at different FFP angles as shown in Fig. 5(b), which is due to various coupled seed power when the seed VCSEL is pumped by different currents [22]. In order to solve this problem, we can equalize the amplified power by reducing the injection current at amplifier and adjusting the pump current at the seed laser. The results are shown in Fig. 6(a). The intensity of

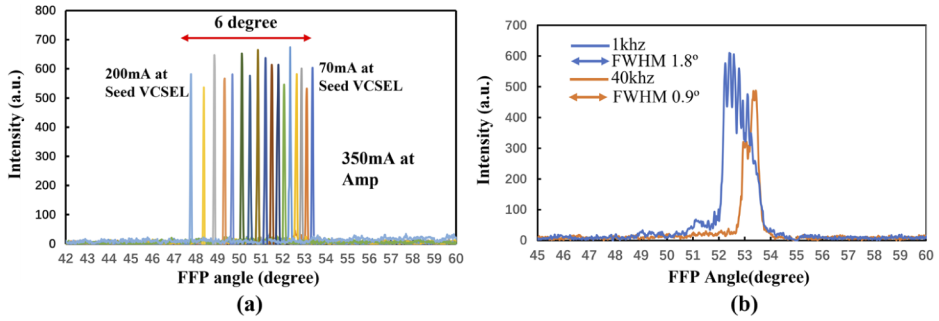

Fig. 6. (a) Equalized FFP with reducing pump current at amplifier. (b) Averaged FFPs under sinusoidal current pumping with a modulation frequency of 1 kHz and 40 kHz.

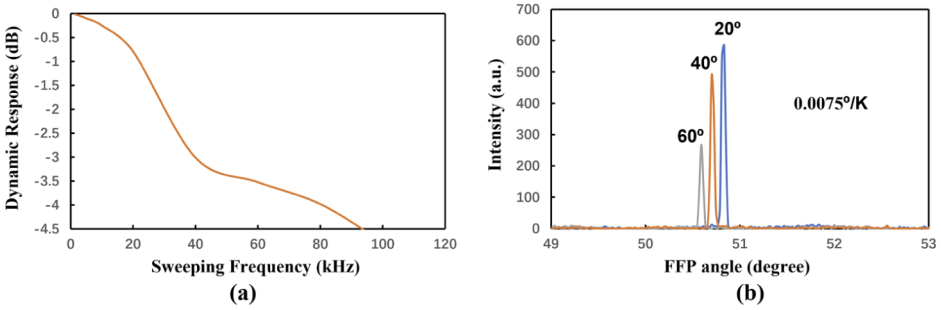

Fig. 7. (a) Dynamic response of beam steering. (b) Temperature dependence of FFP angle.

Optics EXPRESS

the amplified power under steering is equalized at a penalty of 30% reduction in peak power and 3° reduction in beam scanning range.

The scanning speed of the integrated device is also evaluated through applying a sinusoidal modulation current superimposed with DC current at the seed VCSEL and measuring the FFP at different sinusoidal frequencies. Figure 6(b) shows the measured FFPs under sinusoidal current with a modulation frequency of 1 kHz and 40 kHz. Because the modulation speed is much higher than the FFP camera frame rate, time-averaged FFP is observed in the figure. It is noted that the total scanning angle is limited to 1.8° at 1 kHz because of the limited amplitude current of the pulse generator used in the experiment. Increasing the modulation frequency causes reduction in the beam scanning range. Figure 7(a) shows the beam steering range against the modulation frequency. Compared with the mechanical beam steering devices, our integrated device shows a much faster beam steering speed with a 3dB bandwidth of around 40 kHz, which should be large enough for 3D sensing applications with high-frame rates. Figure 7(b) shows the environment temperature dependence of the FFP angle when the VCSEL is injected with a current of 150mA and the amplifier is injected with a current of 350mA. The temperature is controlled through a heater attached to the measurement stage. As we increase the temperature, the FFP angle reduces slightly at a rate of 0.0075°/K. The FFP angle shows weak dependence on the environment temperature because the reduction of FFP angle caused by the wavelength red-shift of the seed laser cancels off with the increase of FFP angle caused by the refractive index change in the amplifier.

5. Conclusion

In summary, we demonstrated a solid-state beam scanner based on surface-grating loaded VCSELs, which shows a record single mode power of 3 W and quasi single mode power of 4W. Compared with the conventional oxide aperture VCSELs, the single mode power is enhanced by 1000 times. Continuous scanning range of 9° with 200 resolution points are also achieved at the same time. Because of the scaling law, by extending the amplifier/scanner length, further increases in the output power can be expected. Also, through better heat sinking and a shorter pulse current below 10 nsec to mitigate the effects of thermal roll-over in the amplifier, a single mode power of over 10 W is achievable. Moreover, 2D beam scanning can also be realized with a 1D array of our integrated device, which was reported very recently. Our experiment shows a potential for solid-state VCSEL beam scanners in VCSEL photonics.

Funding. Japan Science and Technology Agency (#JPMJTR211A).

Disclosures. The authors declare no conflicts of interest.

Data Availability. Data underlying the results presented in this work are not publicly available at this time but may be obtained from the authors upon reasonable request

References

1. F. Koyama, S. Kinoshita, and K. Iga, "Room temperature continuous wave lasing characteristics of a GaAs vertical cavity surface-emitting laser," Appl. Phys. Lett. **55**(3), 221–222 (1989).
2. R. S. Geels, S. W. Corzine, and L. A. Coldren, "InGaAs vertical-cavity surface-emitting lasers," IEEE J. Quantum Electron. **27**(6), 1359–1367 (1991).
3. F. Koyama, "Recent Advances of VCSEL Photonics," J. Lightwave Technol. **24**(12), 4502–4513 (2006).
4. K. Iga, "Vertical-Cavity Surface-Emitting Laser: Its Conception and Evolution," Jpn. J. Appl. Phys. **47**(1), 1–10 (2008).
5. M. A. Taubenblatt, "Optical Interconnects for High-Performance Computing," J. Lightwave Technol. **30**(4), 448–457 (2012).
6. K. Iga, "Surface emitting laser–its birth and generation of new optoelectronics field," IEEE J. Select. Topics Quantum Electron. **6**(6), 1201–1215 (2000).
7. A. Larsson, "Advances in VCSELs for Communication and Sensing," IEEE J. Select. Topics Quantum Electron. **17**(6), 1552–1567 (2011).

Optics EXPRESS

8. H. Moench, R. Conrads, C. Deppe, G. Derra, S. Gronenborn, X. Gu, G. Heusler, J. Kolb, M. Miller, P. Pekarski, J. Pollmann-Retsch, A. Pruijmboom, and U. Weichmann, "High-power VCSEL systems and applications," in *Proceedings of SPIE LASE* (Society of Photo-Optical Instrumentation Engineers, 2015), 2076267
9. K. Iga, "Forty years of vertical-cavity surface-emitting laser: Invention and innovation," Jpn. J. Appl. Phys. **57**(8S2), 08PA01 (2018).
10. A. C. Lehman, D. F. Siriani, and K. D. Choquette, "Two-dimensional electronic beam-steering with implant-defined coherent VCSEL arrays," Electron. Lett. **43**(22), 1202–1203 (2007).
11. D. F. Siriani and K. D. Choquette, "Electronically controlled two-dimensional steering of in-phase coherently coupled vertical-cavity laser arrays," IEEE Photonics Technol. Lett. **23**(3), 167–169 (2011).
12. M. T. Johnsona, D. F. Sirianib, M. P. Tanc, and K. D. Choquette, "Beam steering via resonance detuning in coherently coupled vertical cavity laser arrays," Appl. Phys. Lett. **103**(20), 201115 (2013).
13. M. Dummer, K. Johnson, S. Rothwell, K. Tatah, and M. Hibbs-Brenner, "The role of VCSELs in 3D sensing and LiDAR," in *Proceedings of Optical Interconnects XXI* (International Society for Optics and Photonics,2021), 116920C.
14. J. Doylend, M. Heck, J. Bovington, J. Peters, L. Coldren, and J. Bowers, "Two dimensional free-space beam steering with an optical phased array on silicon-on-insulator," Opt. Express **19**(22), 21595–21604 (2011).
15. S. Chung, H. Abediasl, and H. Hashemi, "A Monolithically Integrated Large-Scale Optical Phased Array in Silicon-on-Insulator CMOS," IEEE J. Solid-State Circuits **53**(1), 275–296 (2018).
16. S. Noda, K. Kitamura, T. Okino, D. Yasuda, and Y. Tanaka, "Photonic-Crystal Surface-Emitting Lasers: Review and Introduction of Modulated-Photonic Crystals," in *IEEE J. Sel. Top. Quantum Electron.*, 23(6), 1–7 (2017).
17. K. Ishizaki, M. D. Zoysa, and S. Noda, "Progress in Photonic-Crystal Surface-Emitting Lasers," Photonics **6**(3), 96–110 (2019).
18. X. Gu, T. Shimada, A. Matsutani, and F. Koyama, "Miniature nonmechanical beam deflector based on bragg reflector waveguide with a number of resolution points larger than 1000," IEEE Photonics J. **4**(5), 1712–1719 (2012).
19. X. Gu, T. Shimada, A. Fuchida, A. Matsutani, A. Imamura, and F. Koyama, "Beam steering in GaInAs/GaAs slow-light Bragg reflector waveguide amplifier," Appl. Phys. Lett. **99**(21), 211107 (2011).
20. X. Gu, T. Shimada, and F. Koyama, "Giant and high-resolution beam steering using slow-light waveguide amplifier," Opt. Express **19**(23), 22675 (2011).
21. M. Nakahama, X. Gu, A. Matsutani, T. Sakaguchi, and F. Koyama, "High Power Non-mechanical Beam Scanner based on VCSEL Amplifier," in *Proceedings of 21st Optoelectron. Commun. Conf. held jointly with 2016 Int. Conf. Photonics Switch*, (IEEE, 2016), pp. 4–6
22. Z. Ho, K. Shimura, K. Kondo, X. Gu, A. Matsutani, and F. Koyama, "High Resolution Active Beam Scanner based on VCSEL Amplifier," in *Proceedings of IEEE Photonics Conference* (IEEE, 2018), pp. 1–2.
23. R. Li, Z. Ho, X. Gu, S. Shinada, and F. Koyama, "Solid-state VCSEL beam scanner with ultra-large field of view and high resolution," in *Optical Fiber Communication Conference* (Optical Society of America, 2021), paper W1D. 3.
24. S. Hu, X. Gu, M. Nakahama, and F. Koyama, "Non-mechanical beam scanner based on VCSEL integrated amplifier with resonant wavelength detuning design," Chin. Opt. Lett. **19**(12), 121403-1 (2021).
25. P. Zhang, C. Liu, M. Xiang, X. Ma, G. Zhao, Q. Lu, J. F. Donegan, and W. Guo, "850 nm GaAs/AlGaAs DFB lasers with shallow surface gratings and oxide aperture," Opt. Express **27**(22), 31225–31234 (2019).
26. A. Hassan, M. Ahmed, M. Nakahama, and F. Koyama, "Theoretical Investigation of Slow-Light VCSEL Amplifier," Journal of Experimental andTheoretical Nanotechnology Specialized Researches **2**(2), 93–104 (2018). https://www.siats.co.uk/wp-content/files_mf/4mostafa_ahmed_revised83.pdf
27. S. Hu, A. Hassan, X. Gu, M. Nakahama, and F. Koyama, "Surface grating loaded VCSEL with single mode power of over 80 mW," IEICE Electron. Expr. **18**(11), 20210202-1 (2021).
28. A. Hassan, X. Gu, M. Nakahama, S. Shinada, M. Ahmed, and F. Koyama, "High-power operations of single-mode surface grating long oxide aperture VCSELs," Appl. Phys. Lett. **119**(19), 191103 (2021).
29. S. Hu, A. Hassan, X. Gu, M. Nakahama, and F. Koyama, "Surface grating VCSEL-integrated amplifier/beam scanner with high power and single mode operation," Appl. Phys. Express **14**(6), 062005 (2021).